

## Anisotropy and Interplane Interactions in the Dielectric Response of Graphite

A. G. Marinopoulos,<sup>1</sup> Lucia Reining,<sup>1</sup> Valerio Olevano,<sup>1</sup> and Angel Rubio<sup>2</sup>

<sup>1</sup>Laboratoire des Solides Irradiés, UMR 7642 CNRS/CEA, École Polytechnique, F-91128 Palaiseau, France

<sup>2</sup>Departamento de Física de Materiales, Facultad de Químicas, Universidad del País Vasco/Euskal Herriko Unibertsitatea, Centro Mixto CSIC-UPV/EHU and Donostia International Physics Center (DIPC), 20018 San Sebastián/Donostia, Spain

T. Pichler,<sup>3,4</sup> X. Liu,<sup>3</sup> M. Knupfer,<sup>3</sup> and J. Fink<sup>3</sup>

<sup>3</sup>Institut für Festkörper und Werkstofforschung, Helmholtzstrasse 20, D-01171 Dresden, Germany

<sup>4</sup>Institut für Materialphysik der Universität Wien, Strudlhofgasse 4, A-01090 Wien, Austria

(Received 18 February 2002; published 25 July 2002)

We determined the anisotropic dielectric response of graphite by means of time-dependent density-functional theory and high-resolution valence electron energy-loss spectroscopy. The calculated loss function was in very good agreement with the experiment for a wide range of momentum-transfer orientations with respect to the graphitic basal planes, provided that local-field effects were included in the response. The calculations also showed strong effects of the interlayer Coulomb interaction on the total  $\pi + \sigma$  plasmon. This finding must be taken into account for the explanation of recent loss spectra of carbon nanotube materials.

DOI: 10.1103/PhysRevLett.89.076402

PACS numbers: 81.05.Uw, 71.45.Gm, 73.20.-r, 79.20.Uv

Hexagonal graphite is a layered solid with a weak interplane interaction and very strong in-plane bonding. Therefore, besides having well-known technological applications [1], it is of fundamental interest as an archetype of a quasi-two-dimensional system [2]. Moreover, the recent observation of superconductivity in  $\text{MgB}_2$  [3], which has the graphite structure, and the discovery of carbon nanotubes [4], which are composed of cylindrically wrapped graphene sheets, renew the importance of a complete understanding of the electronic structure and dielectric properties of graphite. It has in fact been predicted that all laminar materials form nanotubes [5].

Experimentally, the dielectric response of graphite has been analyzed by optical [6,7] and, more often, by electron energy-loss spectroscopy (EELS) [8–12]. In the latter case, for a momentum-transfer  $\mathbf{q}$  parallel to the basal plane (perpendicular to the crystallographic  $c$  axis), two characteristic plasmon peaks are observed. They are related to collective excitations of the valence  $\pi$  electrons ( $\pi$  plasmon) and of all valence electrons ( $\pi + \sigma$  plasmon) [9,10]. Little is known, however, about the evolution of the loss spectra for momentum orientations out of the basal plane [7,8]. On the theoretical side, the dielectric,  $\epsilon$ , and loss functions for in-plane  $\mathbf{q}$  and in an energy range (up to 15 eV) which includes the  $\pi$  plasmon were recently determined by tight-binding calculations [13]. Also the optical properties of graphite were calculated from first principles using density functional theory in the local density approximation (LDA) [14]. The anisotropy of  $\epsilon(\mathbf{q} \rightarrow 0)$  with respect to the  $c$  axis was studied but, to our knowledge, no theoretical interpretation of the dependence of the loss spectra upon the orientation of the momentum transfer has ever been attempted [15]. This is, however, an extremely important aspect: As the nanostructures combine in-plane and interplane interactions, it is

timely to discern their respective role. To study this point is far from trivial, since it involves several questions of broad interest: (i) *All* previous theoretical studies presenting results for the dielectric response in graphite have used the independent-particle scheme [13,14], i.e., the random-phase approximation (RPA) ignoring exchange and correlation (XC) effects in the response [18]. Nonetheless, such a neglect is not *a priori* justified. In addition, in view of a long-standing discussion whether the LDA to density-functional theory can successfully predict *ground-state* equilibrium properties of graphite [19], an issue we also seek to resolve here is whether the adiabatic LDA (TDLDA) [20], which neglects long-range XC effects in the response, can reproduce experimentally obtained dielectric functions and *excited-state* properties. (ii) *All* calculations discussing the dielectric response have neglected the crystal local-field effects (LFE), which arise from the spatial inhomogeneity of the electron response [18]. However, perpendicular to the layers graphite is very inhomogeneous and one should therefore assess the importance of LFE; (iii) an analysis of the effect of the inter-layer interaction on spectroscopic properties is still missing. This interaction was recently found to be responsible for a novel collective excitation mode in  $\text{MgB}_2$  [21] and may contribute to the differences in the dielectric response between graphite and single-wall nanotubes (SWNT), and between SWNT and multiwall (MWNT) tubes.

In order to answer the above questions, we have performed *ab initio* calculations of the dielectric and loss functions in an energy range up to 45 eV (i.e., including the higher-frequency  $\pi + \sigma$  plasmon), in the framework of time-dependent density-functional theory [20]. Moreover, we have quantitatively verified our results by carrying out new valence EELS experiments on a graphite single crystal in a purpose-built high-resolution spectrometer [22] which

combines both good energy *and* momentum resolution: 180 meV and  $0.03 \text{ \AA}^{-1}$ , respectively.

Within TDLDA, the full polarizability  $\chi$  is connected to the independent-particle polarizability [23]  $\chi_0$  via

$$\chi = \chi_0 + \chi_0(V_C + f_{xc})\chi, \quad (1)$$

where  $V_C$  is the bare Coulomb interaction and the XC kernel  $f_{xc}$  is the functional derivative of the LDA XC potential with respect to the electron density. Within RPA,  $f_{xc}$  is assumed to be zero. Both approximations treat  $V_C$ , and therefore crystal LFE, exactly. We have carried out TDLDA and RPA calculations [24], and for the range of momentum transfer studied the results are very similar. Therefore mainly the RPA results will be explicitly presented.

The RPA dielectric function for a periodic system reads  $\varepsilon_{\mathbf{G},\mathbf{G}'}(\mathbf{q}) = \delta_{\mathbf{G},\mathbf{G}'} - V_C(\mathbf{q} + \mathbf{G})\chi_{0\mathbf{G},\mathbf{G}'}(\mathbf{q})$ , with  $\mathbf{q}$  in the first Brillouin zone and  $\mathbf{G}, \mathbf{G}'$  are reciprocal lattice vectors. The loss function for a transferred momentum ( $\mathbf{q} + \mathbf{G}$ ) is given by  $-\text{Im}[\varepsilon_{\mathbf{G},\mathbf{G}}^{-1}(\mathbf{q})] = -\text{Im}[V_C(\mathbf{q} + \mathbf{G})\chi_{\mathbf{G},\mathbf{G}}(\mathbf{q})]$ . In an inhomogeneous system the off-diagonal elements of  $\varepsilon_{\mathbf{G},\mathbf{G}'}$  contribute to the matrix inversion. The approximation  $\varepsilon_{\mathbf{G},\mathbf{G}}^{-1}(\mathbf{q}) \approx 1/\varepsilon_{\mathbf{G},\mathbf{G}}(\mathbf{q})$  neglects the inhomogeneity of the response, i.e., the LFE.

We have determined the loss function with and without LFE for  $|\mathbf{q}| = 0.25 \pm 0.03 \text{ \AA}^{-1}$  ( $\mathbf{G} = \mathbf{0}$ ), and for angles between  $\mathbf{q}$  and the  $c$  axis of  $\Theta = 90^\circ$  (in-plane), and for  $\Theta = 77^\circ$ ,  $\Theta = 45^\circ$ ,  $\Theta = 30^\circ$ , and  $\Theta = 0^\circ$  (parallel to the  $c$  axis). Figure 1 shows the results for the loss function, and Fig. 2 contains the imaginary and real parts of the macroscopic dielectric function,  $\varepsilon_M$ , which is defined as  $\varepsilon_M(\mathbf{q}) = 1/\varepsilon_{\mathbf{0},\mathbf{0}}^{-1}(\mathbf{q})$ . The dashed lines are calculated without, continuous lines including LFE. The dotted lines are the experimental results. The upper panel in Fig. 1 shows that LFE are very small for the in-plane polarization. With or without them, both plasmon positions at 7.2 eV ( $\pi$  plasmon) and 28 eV ( $\pi + \sigma$  plasmon) and line shapes are in very good agreement with the experiment. As seen from Fig. 2, and in agreement with previous results [9,10,25], the  $\pi$  and  $\pi + \sigma$  plasmons correspond to zeros of  $\text{Re}[\varepsilon_M]$  stemming from strong nonvertical interband transitions  $\pi \rightarrow \pi^*$  in the energy range 2–5 eV, and (primarily)  $\sigma \rightarrow \sigma^*$  transitions beyond 10 eV, respectively.

When  $\mathbf{q}$  is oriented closer to the  $c$  direction (lower panels), there are considerable changes in the loss function due to the important anisotropy of  $\varepsilon_M$ . Figure 2 shows that in the low-frequency region (0–10 eV) the oscillator strength associated with the  $\pi \rightarrow \pi^*$  interband transitions is strongly decreased (almost vanishes) for  $\Theta = 0^\circ$ . As a consequence,  $\text{Re}[\varepsilon_M]$  flattens and does not have a zero crossing any more: The  $\pi$  plasmon is progressively displaced to lower frequencies for smaller  $\Theta$  and essentially disappears (Fig. 1). For  $\Theta = 0^\circ$ , oscillator strength is maintained for the  $\pi \rightarrow \sigma^*$  and  $\sigma \rightarrow \pi^*$  transitions between 10 and 17 eV and also transferred to higher energies contributing to a small value for  $\text{Im}[\varepsilon_M]$ . As a consequence, the corresponding contribution to  $\text{Re}[\varepsilon_M]$  is nega-

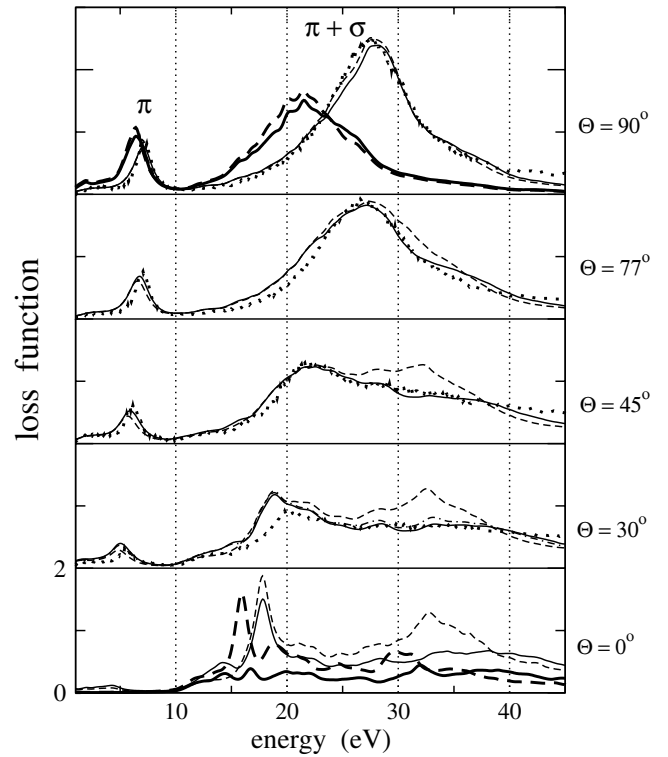


FIG. 1. Calculated and measured loss function for different orientation angles between the momentum-transfer  $\mathbf{q}$  (for  $q = 0.25 \text{ \AA}^{-1}$ ) and the  $c$  axis direction. Dashed lines are obtained without, continuous lines including LFE within the RPA. The dot-dashed curve in the  $\Theta = 30^\circ$  spectrum (hardly distinguishable from the continuous one) is a TDLDA result (with LFE). A broadening of 0.5 eV was used. The thick lines denote the results with the double interlayer spacing. The experimental results are indicated by the dotted lines.

tive in a more restricted frequency region. For smaller  $\Theta$ , a continuum of electron-hole excitations develops in the loss function in a very extended frequency range (from 18 eV up to and beyond 45 eV). The  $\pi + \sigma$  plasmon peak is shifted to lower energies: at 22 and 19 eV for  $\Theta = 45^\circ$  and  $\Theta = 30^\circ$ , respectively. Since at these energies the total  $\pi + \sigma$  plasmon is immersed in the electron-hole continuum, the peaks are much less sharp (especially for  $\Theta = 45^\circ$ ). For  $\Theta = 0^\circ$ , there is a sharper plasmon peak at about 18 eV, followed by the continuum.

The importance of LFE continuously increases with decreasing  $\Theta$ . The positions of the existing plasmon peaks are not modified by LFE, but the line shape of the electron-hole continuum is drastically altered. The calculations without LFE for  $\Theta = 0^\circ$  (dashed line in Fig. 1) miss the shoulder in the loss function at about 14 eV and display a distinct peak in the energy region 32–34 eV. Instead, LFE mix the interband transitions at that energy with the ones at higher frequencies. This leads to a more diffuse shape for the loss function (20–45 eV).

The experimental measurements in Fig. 1 are in very good agreement with the calculated results especially for

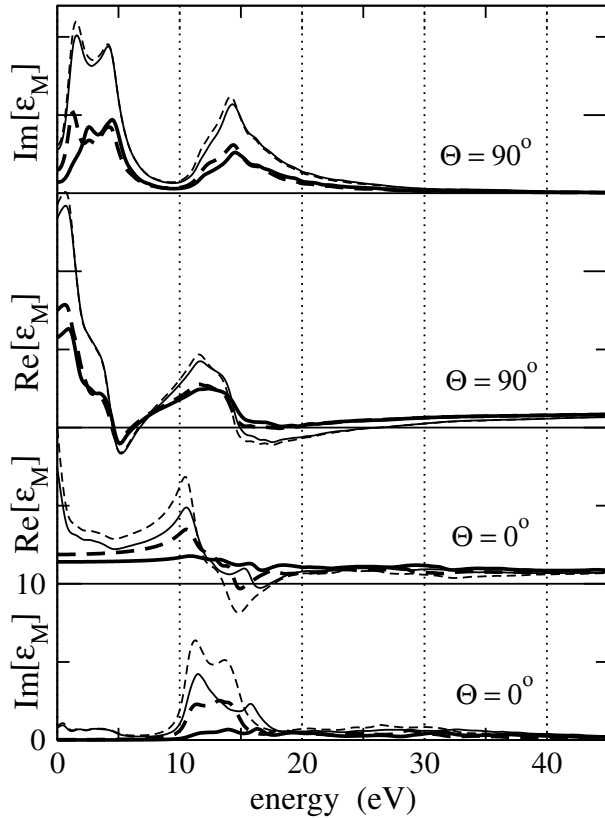


FIG. 2. Calculated  $\text{Im}[\epsilon_M]$  and  $\text{Re}[\epsilon_M]$  for two different  $\mathbf{q}$  polarizations (in-plane  $\Theta = 90^\circ$  and perpendicular-to-plane  $\Theta = 0^\circ$ ). Dashed lines are obtained without, continuous lines including LFE. A broadening of 0.5 eV was used. The thick lines denote the results with the double interlayer spacing.

larger angles and support the theoretical predictions regarding the changes in the line shape of the loss function with out-of-plane  $\mathbf{q}$  orientations ( $\Theta \neq 90^\circ$ ). Furthermore, the agreement between theory and experiment is better when LFE are included. Only for  $\Theta = 30^\circ$  some discrepancy exists between theory and experiment (most notably in the 17–20 eV range) which still persists even if the TDLDA result (dot-dashed curve in Fig. 1) is taken. It is, at present, impossible to quantify the relative importance of the effects which could be responsible for such discrepancy: First, the experimental error in the angle  $\Theta$  can be as large as  $3^\circ$  for lower  $\Theta$ , leading to an estimated uncertainty of 1 eV in the  $\pi + \sigma$  plasmon position. Second, the neglect of long-range XC effects, absent in TDLDA, might be less justified for smaller angles where screening is weak. For  $\Theta = 0^\circ$ , we can compare our calculated results to the earlier experimental work of Ref. [8], which was performed in the optical limit and at about  $\Theta = 10^\circ$ . The experiment qualitatively confirms the much decreased intensity in the low-energy region, the sharpening of the peak just below 20 eV, and the absence of any additional peak on top of the continuum around 32 eV (a peak that again erroneously is predicted by the theory if LFE are neglected). The above comparisons demonstrate that *LFE*

are important for out-of-basal-plane  $\mathbf{q}$  orientations. This finding can be explained from the strong inhomogeneity of the valence electron density in graphite due to the stacking of the widely spaced graphene layers along the  $c$  axis.

One might wonder to which extent these layers behave as isolated systems in their dielectric response. Several findings in the present work are consistent with such a picture: first, the very small dispersion with increasing magnitude of  $\mathbf{q}$  which we find in our calculated  $\Theta = 0^\circ$  results (not shown here). Second, the almost vanishing oscillator strength at low energies ( $< 10$  eV) for  $\Theta = 0^\circ$  is a consequence of the fact that the matrix elements in  $\text{Im}[\epsilon_M]$  for the  $\pi \rightarrow \pi^*$  transitions are very small. Such a behavior is consistent with nearly isolated graphene layers interacting weakly with each other and causes the disappearance of the  $\pi$  plasmon. Indeed, for the case of an isolated layer, the above transitions are symmetry forbidden from 2D selection rules and  $\text{Im}[\epsilon_M]$  is exactly zero [25]. A third indication that turning  $\mathbf{q}$  around (towards smaller  $\Theta$ ) brings us from an extended to a more confined system is the fact that the  $\pi + \sigma$  plasmon moves as much as 10 eV to lower energies. This means, since the energy range of the interband transitions is essentially unchanged (see Fig. 2), that the loss function becomes much more similar to the imaginary part of  $\epsilon_M$  (with LFE included). In fact, in a completely isolated system  $\text{Im}[\epsilon_M]$  and the loss function coincide.

In order to elucidate in more detail the effects of the interlayer interaction, we have also carried out analogous calculations doubling the interlayer separation. The results for  $\Theta = 90^\circ$  and  $\Theta = 0^\circ$  are shown as thick dashed (no LFE) and thick solid (including LFE) lines in Figs. 1 and 2. First, it can be seen (Fig. 2) that for  $\Theta = 0^\circ$  the oscillator strength is zero at lower energies ( $< 10$  eV) in perfect accordance with 2D selection rules applicable for an isolated graphene layer [25]. Without LFE, the  $\text{Im}[\epsilon_M]$  shows, apart from a scaling factor due to the volume change, only minor changes (except in the low-frequency range for  $\Theta = 0^\circ$ ) when the interplane spacing is increased. This means that there is only a weak interaction through the electronic structure since in the absence of LFE the dielectric response is governed solely from the independent band to band transitions. On the other hand, when LFE are included (i.e., when the bare Coulomb interaction is allowed to mix transitions) there is a considerable change in  $\text{Im}[\epsilon_M]$  for  $\Theta = 0^\circ$  and  $\text{Re}[\epsilon_M]$ , for  $\Theta = 0^\circ$ , gets close to 1 (very weak screening) over the entire spectral range. In the loss function for  $\Theta = 0^\circ$ , when LFE are neglected the plasmon peak is shifted to lower frequencies. When LFE are included, the loss function does not display any discernible plasmon peaks and becomes very similar to  $\text{Im}[\epsilon_M]$ , i.e., to the absorption spectrum, due to the weakness of screening.

In plane, the  $\pi$  plasmon does not show drastic changes when the spacing is doubled; there is a small increase of its intensity and also a small shift to lower frequencies. In contrast, the  $\pi + \sigma$  plasmon shifts to lower frequencies by as much as 7 eV, and its intensity decreases. This redshift

of both plasmons should be a generic behavior for any layered system. Its origin must be traced to the halving of  $\text{Im}[\epsilon_M]$  and the concomitant weaker screening when the interlayer spacing (hence, the total volume) is doubled. Consequently, the positions of zeros of  $\text{Re}[\epsilon_M]$  undergo a redshift and, therefore, the frequencies of the collective excitations are decreased (far more notably of the  $\pi + \sigma$  plasmon). LFE continue to be weak. Interestingly, both the  $\pi$  and  $\pi + \sigma$  plasmon peaks cannot be identified any longer as simply due to a zero of  $\text{Re}[\epsilon_M]$ , because of the redshift of the position of the zero which makes it fall into the electron-hole continuum. Rather, the peak positions are now determined by a part of the spectrum where  $\text{Im}[\epsilon_M]$  decreases, and  $\text{Re}[\epsilon_M]$  increases monotonically, a situation which can give rise to significant peaks in the loss spectra, as has also been found in other systems [26].

The above important effects of the interlayer interaction on the  $\pi + \sigma$  plasmon should be taken into account in analyses of the dielectric response of carbon nanotubes: Energy shifts of the  $\pi + \sigma$  plasmon of similar magnitude have been observed recently in EELS experiments on polycrystalline bulk samples of carbon SWNT bundles [27] and MWNTs [28]. The  $\pi + \sigma$  plasmon is, hence, a key quantity to study in order to understand the role of intrawall and interwall interactions in the loss spectra.

In conclusion, the ensuing overall good agreement between the RPA and the TDLDA calculations and experiment demonstrates that XC effects have a small effect in the loss function for a wide range of momentum-transfer orientations and can be neglected, except perhaps for small  $\Theta$  where further work beyond TDLDA may be necessary for more definitive conclusions. LFE are, instead, *crucial* in order to obtain unbiased results. Moreover, we have shown how features of an isolated system show up in the response perpendicular to the planes. However, there is still a strong interplane interaction in graphite. It does not stem from the electronic structure but from the interplane Coulomb interaction. This is intuitive, since in every spectroscopic measurement the sample is *excited*, which means that additional medium- or long-range interactions show up with respect to the *ground state*. We analyzed the important consequences of these interactions, especially for the  $\pi + \sigma$  plasmon for both perpendicular and in-plane  $\mathbf{q}$  orientations, and we argued that they must be taken into account for the interpretation of the loss spectra of carbon nanotubes. Since our results are explained by general arguments, we claim that the impressive sensitivity of the higher valence plasmon to both the interplane separation and to the polarization makes this spectral feature an excellent candidate for the study of any layered, tubelike, or fullerene-like material.

This work was supported by the EC-RTN program NANOPHASE (Contract No. HPRN-CT-2000-00167). A.R. acknowledges support from the Ecole Polytechnique during a sabbatical leave, Iberdrola, and DGES. T.P. thanks the ÖAW for an APART grant. Computer time was granted by IDRIS (Project No. 544).

- [1] See, e.g., M.S. Dresselhaus and G. Dresselhaus, *Adv. Phys.* **30**, 139 (1981).
- [2] J. Gonzalez, F. Guinea, and M. A. H. Vozmediano, *Phys. Rev. B* **63**, 134421 (2001).
- [3] J. Nagamatsu *et al.*, *Nature (London)* **410**, 63 (2001).
- [4] *Carbon Nanotubes: Synthesis, Structure, Properties, and Applications*, edited by M. S. Dresselhaus, G. Dresselhaus, and Ph. Avouris (Springer-Verlag, Berlin, 2001).
- [5] S. G. Louie, in *The Chemical Physics of Fullerenes*, edited by W. Andreoni (Kluwer, Dordrecht, 1996), p. 419; A. Zettl, *Adv. Mater.* **8**, 443 (1996), and references therein.
- [6] E. A. Taft and H. R. Philipp, *Phys. Rev.* **138**, A197 (1965).
- [7] R. Klucker, M. Skibowski, and W. Steinmann, *Phys. Status Solidi (b)* **65**, 703 (1974).
- [8] K. Zeppenfeld, *Z. Phys.* **211**, 391 (1968).
- [9] K. Zeppenfeld, *Z. Phys.* **243**, 229 (1971).
- [10] U. Büchner, *Phys. Status Solidi (b)* **81**, 227 (1977).
- [11] N. Papageorgiou, M. Portail, and J. M. Layet, *Surf. Sci.* **454-456**, 462 (2000).
- [12] M. Vos *et al.*, *Phys. Rev. B* **63**, 033108 (2001).
- [13] C. S. Huang, M. F. Lin, and D. S. Chuu, *Solid State Commun.* **103**, 603 (1997); M. F. Lin, C. S. Huang, and D. S. Chuu, *Phys. Rev. B* **55**, 13 961 (1997).
- [14] R. Ahuja *et al.*, *Phys. Rev. B* **55**, 4999 (1997).
- [15] Anisotropy effects also show up in the measured [16] and calculated electron lifetimes [17].
- [16] G. Moos *et al.*, *Phys. Rev. Lett.* **87**, 267402 (2001).
- [17] C. Spataru *et al.*, *Phys. Rev. Lett.* **87**, 246405 (2001).
- [18] The inverse dielectric matrix of graphite was also calculated in Refs. [12,17] as an ingredient for other quantities, however, without being discussed.
- [19] M. C. Schabel and J. L. Martins, *Phys. Rev. B* **46**, 7185 (1992); J. C. Charlier, X. Gonze, and J. P. Michenaud, *Europhys. Lett.* **28**, 403 (1994).
- [20] E. Runge and E. K. U. Gross, *Phys. Rev. Lett.* **52**, 997 (1984); E. K. U. Gross and W. Kohn, *Phys. Rev. Lett.* **55**, 2850 (1985); G. Onida, L. Reining, and A. Rubio, *Rev. Mod. Phys.* **74**, 601 (2002).
- [21] W. Ku *et al.*, *Phys. Rev. Lett.* **88**, 057001 (2002).
- [22] J. Fink, *Adv. Electron. Electron Phys.* **75**, 121 (1989), and references therein.
- [23] M. Petersilka, U. J. Gossmann, and E. K. U. Gross, *Phys. Rev. Lett.* **76**, 1212 (1996).
- [24] We have used norm-conserving pseudopotentials [N. Troullier and J. L. Martins, *Phys. Rev. B* **43**, 1993 (1991)], a plane-wave basis, and up to 7290  $\mathbf{k}$ -points for the Brillouin-zone sums, which gave converged results for frequencies above 1 eV. An investigation of low-frequency (e.g., infrared) plasmons in the loss spectrum of this semimetal would require an improved treatment of intraband transitions and is beyond the scope of the present work.
- [25] F. Bassani and G. Pastori Parravicini, *Nuovo Cimento* **50**, 95 (1967).
- [26] N. Vast *et al.*, *Phys. Rev. Lett.* **88**, 037601 (2002); I. Campillo, A. Rubio, and J. M. Pitarke, *Phys. Rev. B* **59**, 12 188 (1999).
- [27] T. Pichler *et al.*, *Phys. Rev. Lett.* **80**, 4729 (1998).
- [28] T. Pichler *et al.* *AIP Conf. Proc.* **486**, 346 (1999); (unpublished).